Title
Probing Hydrogen Bonding Interactions to Iron-Oxido/Hydroxido Units by 57Fe Nuclear Resonance Vibrational Spectroscopy

Journal
Angewandte Chemie International Edition, 57(49)

ISSN
1433-7851

Authors
Weitz, Andrew C
Hill, Ethan A
Oswald, Victoria F
et al.

Publication Date
2018-12-03

DOI
10.1002/anie.201810227

Peer reviewed

HHS Public Access

Author manuscript

Angew Chem Int Ed Engl. Author manuscript; available in PMC 2018 December 03.

Published in final edited form as:

Angew Chem Int Ed Engl. 2018 December 03; 57(49): 16010–16014. doi:10.1002/anie.201810227.

Probing hydrogen bonding interactions to iron-oxido/hydroxido units via ^{57}Fe nuclear resonance vibrational spectroscopy

Andrew C. Weitz[a], **Ethan A. Hill**[b], **Victoria F. Oswald**[b], **Emile L. Bominaar**[a], **A. S. Borovik**[b], **Michael P. Hendrich**[a], and **Yisong Guo**[a]

[a]Department of Chemistry, Carnegie Mellon University, Pittsburgh, PA 15213 (USA)

[b]University of California, Irvine, CA 92697 (USA)

Abstract

Hydrogen bonds (H-bonds) have been shown to modulate the chemical reactivities of iron centers in iron-containing dioxygen-activating enzymes and model complexes. However, few examples are available that investigate how systematic changes on intramolecular H-bonds within the secondary coordination sphere influence specific properties of iron intermediates, such as iron-oxido/hydroxido species. Here, we used ^{57}Fe nuclear resonance vibrational spectroscopy (NRVS) to probe the Fe–O/OH vibrations in a series of Fe^{III}–hydroxido and $Fe^{IV/III}$–oxido complexes with varying H-bonding networks but having similar trigonal bipyramidal primary coordination spheres. The data show that even subtle changes in the H-bonds to the Fe–O/OH units result in significant changes in their vibrational frequencies, thus demonstrating the utility of NRVS in studying the effect of the secondary coordination sphere to the reactivities of iron complexes.

Graphical Abstract

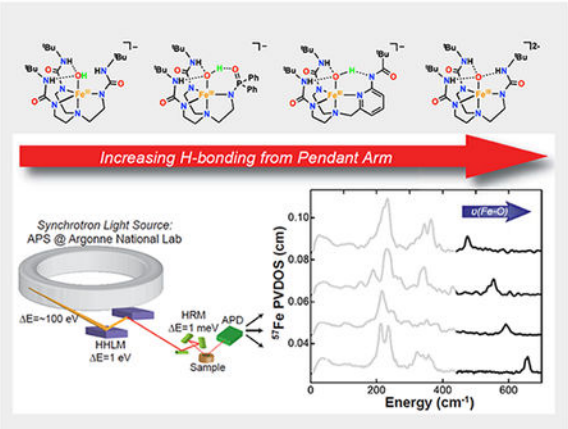

Hydrogen bond strength to iron(III)-oxido/hydroxido (Fe^{III}-O/OH) units in nonheme iron complexes is revealed by ^{57}Fe nuclear resonance vibrational spectroscopy through the detection of Fe^{III}-O/OH stretching vibrations, thus providing a methodology to elucidate the influence of

Supporting information for this article is given via a link at the end of the document.

hydrogen bonds in the secondary coordination sphere to the stability of Fe^{III}-O/OH units, and potentially connecting it to the reactivities of Fe^{IV}-O units towards substrates.

Keywords

hydrogen bonds; non-heme iron-oxo/hydroxo complexes; ^{57}Fe nuclear resonance vibrational spectroscopy; secondary coordination sphere; C-H activation

The primary and secondary coordination sphere interactions to the metal centers of metalloenzymes are strong determinants of chemical properties that promote a wide range of function.[1–6] While the primary coordination sphere ligands and their geometry tune the metal redox potentials for substrate reactivity, secondary coordination sphere interactions, such as H-bonds, have been shown also to affect function.[7,8] Among dioxygen-activating enzymes, H-bonds between nearby residues and metal bound oxygen species can influence function to support a variety of reaction pathways. For instance, in heme-containing proteins proximal residues to the heme center stabilize the binding of O_2 in hemoglobins and myoglobins.[9–14] In contrast, H-bonds facilitate O–O bond cleavage in heme peroxidases and cytochrome P450 dependent enzymes.[15–20] In nonheme iron enzymes, H-bonding networks have been shown to affect the stabilization of the iron bound O_2 intermediate, thereby lowering the energetic barriers for O_2 activation[21–23] and substrate oxidation.[24,25] H-bonds are also proposed to affect the reactivity of high valent Fe^{IV}–oxido intermediates for the homolytic cleavage of C–H bond and subsequent stabilization of the resultant Fe^{III}–OH species.[26,27]

These examples from biology have inspired the development of synthetic systems to further investigate the influences of intramolecular H-bonds on the properties of metal ions. For dioxygen binding and activation, synthetic systems have been employed to systematically alter the ligand structure to correlate changes between the primary coordination sphere and H-bonding networks within the secondary coordination sphere of metal center(s).[28–30] Because of the relationships to protein intermediates, $Fe^{IV/III}$–oxido and Fe^{III}–hydroxido complexes have been utilized to probe the relationship between H-bonds to the iron-oxido/hydroxido units and their reactivity.[15,31–34] However, there are still few examples that examine how systematic changes within the secondary coordination sphere affect specific properties of Fe complexes.

Here we describe the effects of intramolecular H-bonds on the vibrational properties of monomeric Fe–O(H) complexes. We have prepared a series of Fe^{III}–hydroxido and $Fe^{IV/III}$–oxido complexes with varying H-bonding networks but similar trigonal bipyramidal primary coordination spheres. These structural properties were achieved using a set of tripodal ligands that contain at least two mono-deprotonated urea groups (Figure 1): the ligands differ by the functional group on the third tripodal arm. The symmetric $[H_3buea]^{3-}$ contains a third deprotonated urea group, whereas $[H_2pout]^{3-}$ and $[H_2bupa]^{3-}$ have phosphinic amido and carboxyamidopyridyl groups, respectively. Characterization of the Fe^{III} complexes by electron paramagnetic resonance (EPR) and Mössbauer spectroscopies (Table S3, Figures S2–6) showed that all ligands provide similar electronic environment to the Fe center. ^{57}Fe nuclear resonance vibrational spectroscopy (NRVS)[35–37] was used to measure the Fe–O(H)

vibration of each complex to assess the strength of H-bond between the functional group on the third tripodal arm and the Fe–O(H) unit. The advantage of NRVS over other vibrational spectroscopies is that it detects all vibrational modes with iron motion, thus having high specificity and sensitivity to the iron centers. Because the Fe complexes have similar electronic structures and primary coordination spheres, we reasoned that any change in the Fe–O(H) vibrations would be attributed to the strength of this single intramolecular H-bond.

The NRVS derived ^{57}Fe partial vibrational density of states (PVDOS) spectrum of $[Fe^{III}\{H_3buea\}(O)]^{2-}$ recorded on solid powder is shown in Figure 2 (Data measured on solid powder and in frozen solution for the same complex do not show significant difference. For example, please see Figure S9 for the results on $[Fe^{IV}\{H_3buea\}(O)]^{-}$). The major spectral features are separated into three regions. In the high-energy region above 450 cm^{-1}, only one intense peak is observed at 660 cm^{-1} [38] and is assigned as $\nu(Fe^{III}–O)$ stretching mode based on the similar energy obtained for this vibration from FTIR measurements ($\nu(Fe^{III}–O)$ = 670 cm^{-1}).[39] The strongest ^{57}Fe PVDOS features are observed in the low-energy region (100–300 cm^{-1}), where two peaks are observed with frequencies of 213 cm^{-1} and 236 cm^{-1}. In the mid-energy region (300–450 cm^{-1}), a broad feature with distinguishable peaks at 324 and 361 cm^{-1} is observed. These ^{57}Fe PVDOS features are assigned mainly to N-Fe-N/OFe-N bending modes (100–300 cm^{-1}) and Fe–N stretching modes (300–450 cm^{-1}) based on DFT calculations (infra vide). Similar assignments have been reported for the NRVS data of another trigonal bipyramidal Fe^{IV}–oxido complex, $[Fe^{IV}\{TMGtren\}(O)]^{2+}$.[40]

DFT calculations (BP86/TZVP) provided additional support of the spectral assignments. The DFT optimized structure closely resembled the molecular structure of $[Fe^{III}\{H_3buea\}(O)]^{2-}$ obtained from X-ray diffraction methods (Table S4, Figure S8), which showed a C_3 symmetric species. Based on the DFT derived structure, the calculated ^{57}Fe PVDOS spectrum reproduced the experimental spectrum well (Figure 2a) to allow assignment of the spectral features to specific vibrational modes. The major vibrational modes of the $[Fe^{III}\{H_3buea\}(O)]^{2-}$ complex can be explained by the normal modes of vibration of a simplified $OFe(X_3)(YZ_3)$ type molecule with C_{3v} symmetry. The normal modes derived from DFT frequency calculations are listed in Figure S7, selected modes and the corresponding assignments are presented in Figure 2b. In particular, the DFT calculated $\nu(Fe^{III}–O)$ stretching mode ($\nu_{12}(A_1)$ mode in C_{3v}) showed a strong ^{57}Fe PVDOS intensity at 638 cm^{-1}, consistent with the experimental observation (see the supporting information for more analysis).

Upon protonation of the Fe^{III}–oxido complex to form $[Fe^{III}\{H_3buea\}(OH)]^{-}$, the ^{57}Fe PVDOS spectrum obtained on solid powder (Figure 3a) still consisted of three major features with intensities similar to those of the $[Fe^{III}\{H_3buea\}(O)]^{2-}$ spectrum, indicating similar overall geometries for the two complexes. However, one feature has shifted to a significantly lower energy (660 to 477 cm^{-1}). When compared with the spectrum measured on the isotopically labeled complex $[Fe^{III}\{H_3buea\}(^{18}OH)]^{-}$ (Figure 3a dashed trace), a 15 cm^{-1} red shift of the band at 477 cm^{-1} to 462 cm^{-1} was observed, identifying this feature as belonging to the $\nu(Fe^{III}–OH)$ vibration ($\Delta\nu(^{16}O/^{18}O)$ = 20 cm^{-1} based on Hook's law). The ~200 cm^{-1} red shift in the Fe–O stretching frequency from $\nu(Fe^{III}–O)$ to $\nu(Fe^{III}–OH)$ is

associated with the significant elongation of Fe–O bond distance from 1.813(3) Å to 1.932(2) Å, which was determined from the XRD derived molecular structures of the two complexes (Table S4).[39,41] DFT calculations reproduced this difference in Fe–O bond length (1.81 Å for Fe^{III}–O and 1.95 Å for Fe^{III}–OH) and the $^{16}O/^{18}O$ isotope shift on ν(Fe^{III}–OH) (483 cm^{-1} to 468 cm-1 with $\Delta\nu = 15\ cm^{-1}$, Figure S10). In addition, the longer Fe–OH bond in $[Fe^{III}\{H_3buea\}(OH)]^-$ also results in a shortening of Fe–N_{apical} bond length by 0.1 Å which is consistent with a hydroxido ligand having a weaker trans influence than an oxido ligand.[41] As a consequence, the Fe^{III} center shifts into the equatorial plane formed by the three deprotonated N-donors of $[H_3buea]^{3-}$, which in turn strengthens the Fe–N_{eq} bonds (Table S4). These structural changes were also observed in the NRVS spectra. The peaks in the 300–450 cm^{-1} region were blue shifted by ~10 cm^{-1} in $[Fe^{III}\{H_3buea\}(OH)]^-$ spectrum relative to those of $[Fe^{III}\{H_3buea\}(O)]^{2-}$.

We also used the NRVS detected ν[Fe–O(H)] as a probe to examine the effect of H-bonds on the strength of the Fe^{III}–OH bond. The ^{57}Fe PVDOS spectra of $[Fe^{III}\{H_2pout\}(OH)]^-$ and $[Fe^{III}\{H_2bupa\}(OH)]^-$ measured on frozen solutions are shown in Figures 3b,c. Together with $[Fe^{III}\{H_3buea\}(OH)]^-$, these complexes represent a series of Fe^{III}–OH species that are structurally nearly identical except for a single intramolecular H-bond (*vida supra*, Figure 1). In $[Fe^{III}\{H_3buea\}(OH)]^-$, the hydroxido ligand is not a H-bond donor and only two H-bonds are formed. However, in $[Fe^{III}\{H_2pout\}(OH)]^-$ and $[Fe^{III}\{H_2bupa\}(OH)]^-$ the hydroxido ligand can be a H-bond donor to form a third H-bond (OH…X (X = O, N^-), Figures 1 and S8). The NRVS spectra reflect these differences within the secondary coordination spheres: the observed ν[Fe-OH] were located at 556 cm^{-1} for $[Fe^{III}\{H_2pout\}(OH)]^-$ and at 594 cm^{-1} for $[Fe^{III}\{H_2bupa\}(OH)]^-$. Compared to $[Fe^{III}\{H_3buea\}(OH)]^-$, the vibrations represent a blue shift of 79 cm^{-1} for the former complex and 117 cm^{-1} for the latter complex. These assignments were confirmed by DFT calculations (Figures S11-S12).

The energy increases of the Fe–OH vibrations correlate with a strengthening of the Fe–OH bond, which we attribute to the effect of the additional Fe–OH…X H-bond in $[Fe^{III}\{H_2pout\}(OH)]^-$ and $[Fe^{III}\{H_2bupa\}(OH)]^-$. Two lines of evidence support this assertion: (1) The XRD determined Fe–O bond length of 1.893(2) Å for $[Fe^{III}\{H_2pout\}(OH)]^-$ is contracted by 0.046 Å to that found in $[Fe^{III}\{H_3buea\}(OH)]^-$ (Tables S1–S4, Figure S1); and (2) DFT calculations showed that among the three Fe^{III}–OH complexes, $[Fe^{III}\{H_2bupa\}(OH)]^-$ formed the strongest H-bond to afford the shortest OH…N distance, the longest O–H bond, and the shortest Fe-OH bond (Table S4), which results in the highest ν[Fe–O(H)]. The spectral features observed in the lower-energy regions were also considerably more complicated for $[Fe^{III}\{H_2pout\}(OH)]^-$ and $[Fe^{III}\{H_2bupa\}(OH)]^-$, which is consistent with the lower symmetry of these complexes compared to $[Fe^{III}\{H_3buea\}(OH)]^-$.

The correlation between the Fe–O(H) bond length and ν[Fe–O(H)] was extended to include a Fe^{IV} species $[Fe^{IV}\{H_3buea\}(O)]^-$. ν[Fe=O] was reported to be 794 cm^{-1} for this complex from the NRVS data recorded on a frozen solution,[38,42] which is also consistent with the ν[Fe^{IV}=O] of 799 cm^{-1} reported from FTIR measurements.[43] Here, both ^{16}O and ^{18}O isotopomers were further recorded on solid powders (Figure 3e) to confirm its origin as ν[Fe^{IV}=O] vibration with $\Delta\nu(^{16}O/^{18}O) = 30\ cm^{-1}$ ($\Delta\nu = 35\ cm^{-1}$ based on Hook's law).

Figure 4 shows the correlation between the Fe–O(H) bond length and the NRVS-derived ν[Fe–O(H)] based on all 5 complexes studied here, which spans an energy range of ~400 cm $^{-1}$ and bond length differences of ~0.3 Å. This correlation can be explained by Badger's rule, which is an empirical rule correlating bond length with stretching vibrations. The extracted Badger's rule constants from this work are also similar to the ones reported for Fe–O(H) of heme containing systems.[44]

The results described in this study demonstrate the sensitivity of NRVS to probe the properties of Fe–O(H) units within varied secondary coordination spheres. Through a series of synthetic complexes that span Fe^{III}–oxido and Fe^{III}–hydroxido cores, our work revealed effects of protonation and a single H-bond on the Fe^{III}–oxido interaction. Protonation of the oxido ligand in $[Fe^{III}\{H_3buea\}(O)]^{2-}$ to form $[Fe^{III}\{H_3buea\}(OH)]^{-}$ cause a 183 cm^{-1} red shift in energy of the ν[Fe-O]. The Fe–oxido bond character was partially restored by changing the cavity architecture to include a lone H-bond acceptor. With the hydroxido ligand now also serving as a H-bond donor, higher Fe–O(H) vibration energies were observed. For instance, ν[Fe–O(H)] is only red shifted by 66 cm^{-1} for $[Fe^{III}\{H_2bupa\}(OH)]^{-}$ relative to that for $[Fe^{III}\{H_3buea\}(O)]^{2-}$. The interplay between an Fe–OH…X H-bond and ν[Fe–O] was further illustrated in the trend observed for the three Fe^{III}–OH, in which a stronger H-bond correlated with a higher Fe–O vibrational frequency. H-bonding interactions in Fe^{III}–hydroxido complexes can affect chemical transformations that include C–H bond functionalization by high valent Fe^{IV}–oxido intermediates. One factor governing this reactivity is the O–H bond dissociation energy of the Fe^{III}–hydroxido intermediates.[45] The stability of the O–H bond acts as a driving force in C–H bond cleavage. The spectroscopic results presented here provide a quantitative measurement of the modulation of Fe–O bonding and incipient Fe–OH…X H-bond formation and thereby provide a basis from which to understand the stability of O–H bonds in Fe^{III}–OH species. This information in turn can be used to model the reactivity of different complexes involving Fe^{IV}–oxido units and substrates.

Supplementary Material

Refer to Web version on PubMed Central for supplementary material.

Acknowledgements

We thank the U.S. National Institutes of Health (GM050781 to A.S.B., GM49970 to M.P.H.) and the National Science Foundation (CHE-1654060 to Y.G.) for funding support. The NRVS work was performed at the Advanced Photon Source (APS), Argonne National Laboratory (proposal 50088). The use of APS is supported by the Department of Energy. We also thank Drs. M. Hu, J. Zhao, and E. E. Alp for their support in collecting NRVS spectra, Mr. Ruixi Fan and Dr. Jikun Li from Carnegie Mellon University for beamtime assistance.

References

(1). Holm RH; Solomon EI Chem. Rev 2014, 114, 4039. [PubMed: 24758378]
(2). Lu Y; Valentine JS Curr. Opin. Struct. Biol 1997, 7, 495. [PubMed: 9266170]
(3). Lu Y; Berry SM; Pfister TD Chem. Rev 2001, 101, 3047. [PubMed: 11710062]
(4). Liu J; Chakraborty S; Hosseinzadeh P; Yu Y; Tian S; Petrik I; Bhagi A; Lu Y Chem. Rev 2014, 114, 4366. [PubMed: 24758379]

(5). Yu F; Cangelosi VM; Zastrow ML; Tegoni M; Plegaria JS; Tebo AG; Mocny CS; Ruckthong L; Qayyum H; Pecoraro VL Chem. Rev 2014, 114, 3495. [PubMed: 24661096]

(6). Deuss PJ; Denheeten R; Laan W; Kamer PCJ Chem. - A Eur. J 2011, 17, 4680.

(7). Borovik AS Acc. Chem. Res 2005, 38, 54. [PubMed: 15654737]

(8). Cook SA; Borovik AS Acc. Chem. Res 2015, 48, 2407. [PubMed: 26181849]

(9). Springer BA; Sligar SG; Olson JS; Phillips GN Chem. Rev 1994, 94, 699.

(10). Kendrew JC; Bodo G; Dintzis HM; Parrish RG; Wyckoff H; Phillips DC Nature 1958, 181, 662. [PubMed: 13517261]

(11). Kendrew JC; Dickerson RE; Strandberg BE; Hart RG; Davies DR; Phillips DC; Shore VC Nature 1960, 185, 422. [PubMed: 18990802]

(12). Perutz MF; Rossmann MG; Cullis AF; Muirhead H; Will G; North ACT Nature 1960, 185, 416. [PubMed: 18990801]

(13). Shaanan B Nature 1982, 296, 683. [PubMed: 7070513]

(14). Yang J; Kloek AP; Goldberg DE; Mathews FS Proc. Natl. Acad. Sci. U. S. A 1995, 92, 4224. [PubMed: 7753786]

(15). Poulos TL Chem. Rev 2014, 114, 3919. [PubMed: 24400737]

(16). Poulos TL; Freer SST; Alden RA; Edwards SL; Skogland U; Eriksson B; Xuong N; Yonetani T; Kraut J J. Biol. Chem 1980, 2, 575.

(17). Poulos TL; Kraut J J. Biol. Chem 1980, 255, 8199. [PubMed: 6251047]

(18). Schlichting I; Berendzen J; Chu K; Stock AM; Maves SA; Benson DE; Sweet RM; Ringe D; Petsko GA; Sligar SG 2000, 287, 1615.

(19). Nagano S; Poulos TL J. Biol. Chem 2005, 280, 31659. [PubMed: 15994329]

(20). Vidossich P; Fiorin G; Alfonso-Prieto M; Derat E; Shaik S; Rovira C J. Phys. Chem. B 2010, 114, 5161. [PubMed: 20345187]

(21). Jasniewski AJ; Que L Chem. Rev 2018, 118, 2554. [PubMed: 29400961]

(22). Holmes MA; Le Trong I; Turley S; Sieker LC; Stenkamp RE J. Mol. Biol 1991, 218, 583. [PubMed: 2016748]

(23). Brunold TC; Solomon EI J. Am. Chem. Soc 1999, 121, 8288.

(24). Fielding AJ; Lipscomb JD; Que L J. Biol. Inorg. Chem 2014, 19, 491. [PubMed: 24615282]

(25). Kovaleva EG; Rogers MS; Lipscomb JD Biochemistry 2015, 54, 5329. [PubMed: 26267790]

(26). Wong SD; Srnec M; Matthews ML; Liu LV; Kwak Y; Park K; Bell CB; Alp EE; Zhao J; Yoda Y; Kitao S; Seto M; Krebs C; Bollinger JM; Solomon EI Nature 2013, 499, 320. [PubMed: 23868262]

(27). Mitchell AJ; Zhu Q; Maggiolo AO; Ananth NR; Hillwig ML; Liu X; Boal AK Nat. Chem. Biol 2016, 12, 636. [PubMed: 27348090]

(28). Mukherjee J; Lucas RL; Zart MK; Powell DR; Day VW; Borovik AS Inorg. Chem 2008, 47, 5780. [PubMed: 18498155]

(29). Gordon Z; Drummond MJ; Matson EM; Bogart JA; Schelter EJ; Lord RL; Fout AR Inorg. Chem 2017, 56, 4852. [PubMed: 28394119]

(30). Lucas RL; Zart MK; Murkerjee J; Sorrell TN; Powell DR; Borovik AS J. Am. Chem. Soc 2006, 128, 15476. [PubMed: 17132015]

(31). Wallar BJ; Lipscomb JD Chem. Rev 1996, 96, 2625. [PubMed: 11848839]

(32). Solomon EI; Brunold TC; Davis MI; Kemsley JN; Lee SK; Lehnert N; Neese F; Skulan a J.; Yang YS; Zhou J, Chem. Rev 2000, 100, 235. [PubMed: 11749238]

(33). Costas M; Mehn MP; Jensen MP; Que L, Jr. Chem. Rev 2004, 104, 939. [PubMed: 14871146]

(34). Krebs C; Fujimori DG; Walsh CT; Bollinger JMJ Acc. Chem. Res 2007, 40, 484. [PubMed: 17542550]

(35). Sage JT; Paxson C; Wyllie G. R. a; Sturhahn W; Durbin SM; Champion PM; Alp EE; Scheidt WR J. Phys. Condens. Matter 2001, 13, 7707.

(36). Kohn VG; Chumakov AI Hyperfine Interact 2000, 125, 205.

(37). Sturhahn W J. Phys. Condens. Matter 2004, 16, S497.

(38). Note that the NRVS frequencies differ slightly from the previously reported IR frequencies, [39,43] but they are within the resolution of NRVS spectra, which is 8–10 cm^{-1}..

(39). Macbeth CE; Golombek AP; YouJr VG; Yang C; Kuczera K; Hendrich MP; Borovik AS Science 2000, 289, 938. [PubMed: 10937994]

(40). Wong SD; Bell CB; Liu LV; Kwak Y; England J; Alp EE; Zhao J; Que L; Solomon EI Angew. Chemie - Int. Ed 2011, 50, 3215.

(41). MacBeth CE; Gupta R; Mitchell-Koch KR; Young VG; Lushington GH; Thompson WH; Hendrich MP; Borovik AS J. Am. Chem. Soc 2004, 126, 2556. [PubMed: 14982465]

(42). Hill EA; Weitz AC; Onderko E; Romero-Rivera A; Guo Y; Swart M; Bominaar EL; Green MT; Hendrich MP; Lacy DC; Borovik AS J. Am. Chem. Soc 2016, 138, 13143. [PubMed: 27647293]

(43). Lacy DC; Gupta R; Stone KL; Greaves J; Ziller JW; Hendrich MP; Borovik AS J. Am. Chem. Soc 2010, 132, 12188. [PubMed: 20704272]

(44). Green MT J. Am. Chem. Soc 2006, 128, 1902. [PubMed: 16464091]

(45). Mayer JM Acc. Chem. Res 2011, 44, 36. [PubMed: 20977224]

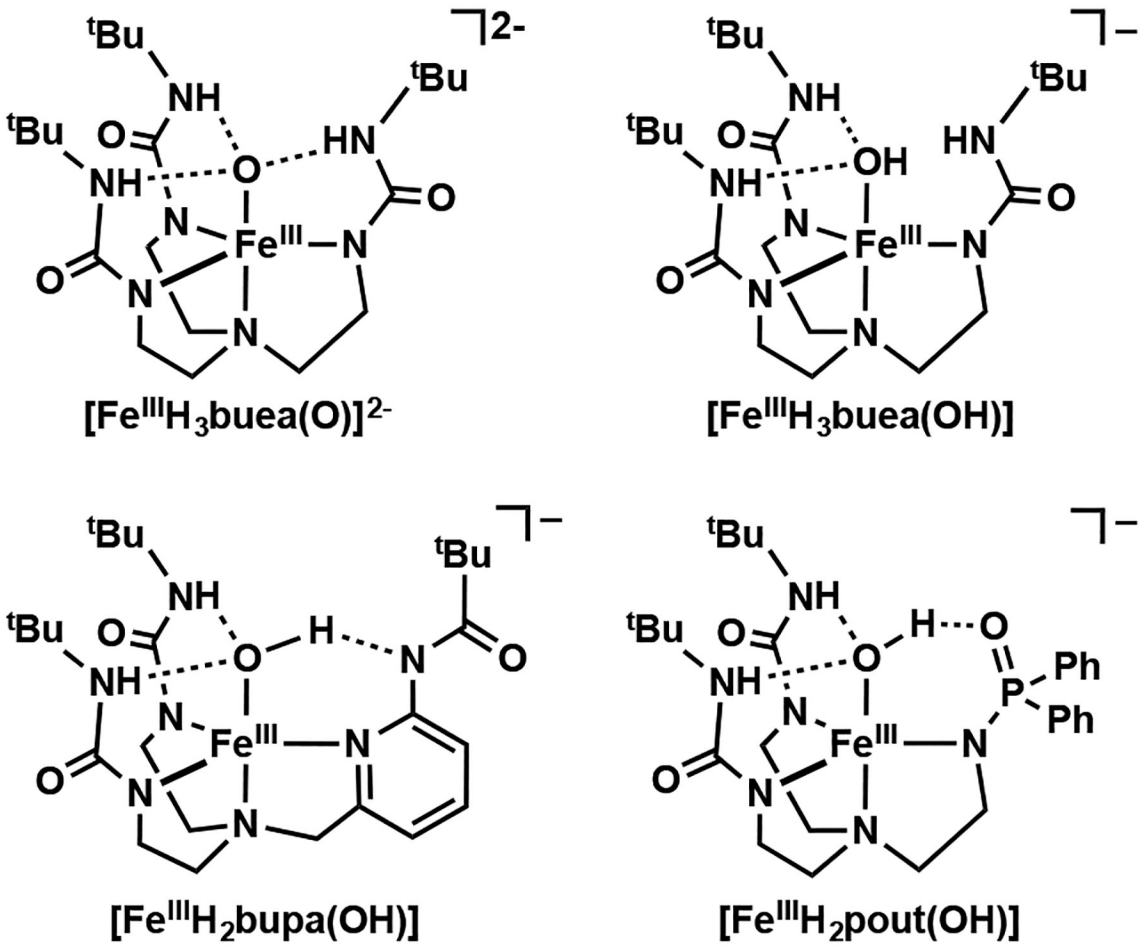

Figure 1.
Structures of Fe^{III} complexes studied by ^{57}Fe NRVS.

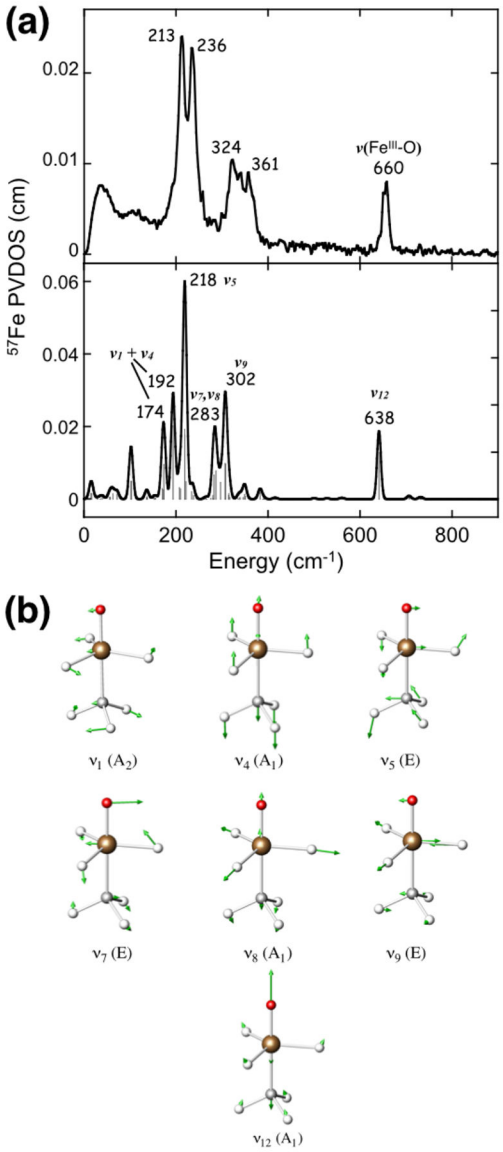

Figure 2.

^{57}Fe PVDOS spectra of [Fe^{III}{H_3buea}(O)]$^{2-}$ and the vibrational mode assignments. (a): the experimental derived (upper trace) and the DFT predicted (lower trace) spectra; (b): the selected mode pictures and the corresponding irreducible representations from a C_{3v} OFe(X_3)(YZ_3) molecule calculated by DFT (see Figure S7).

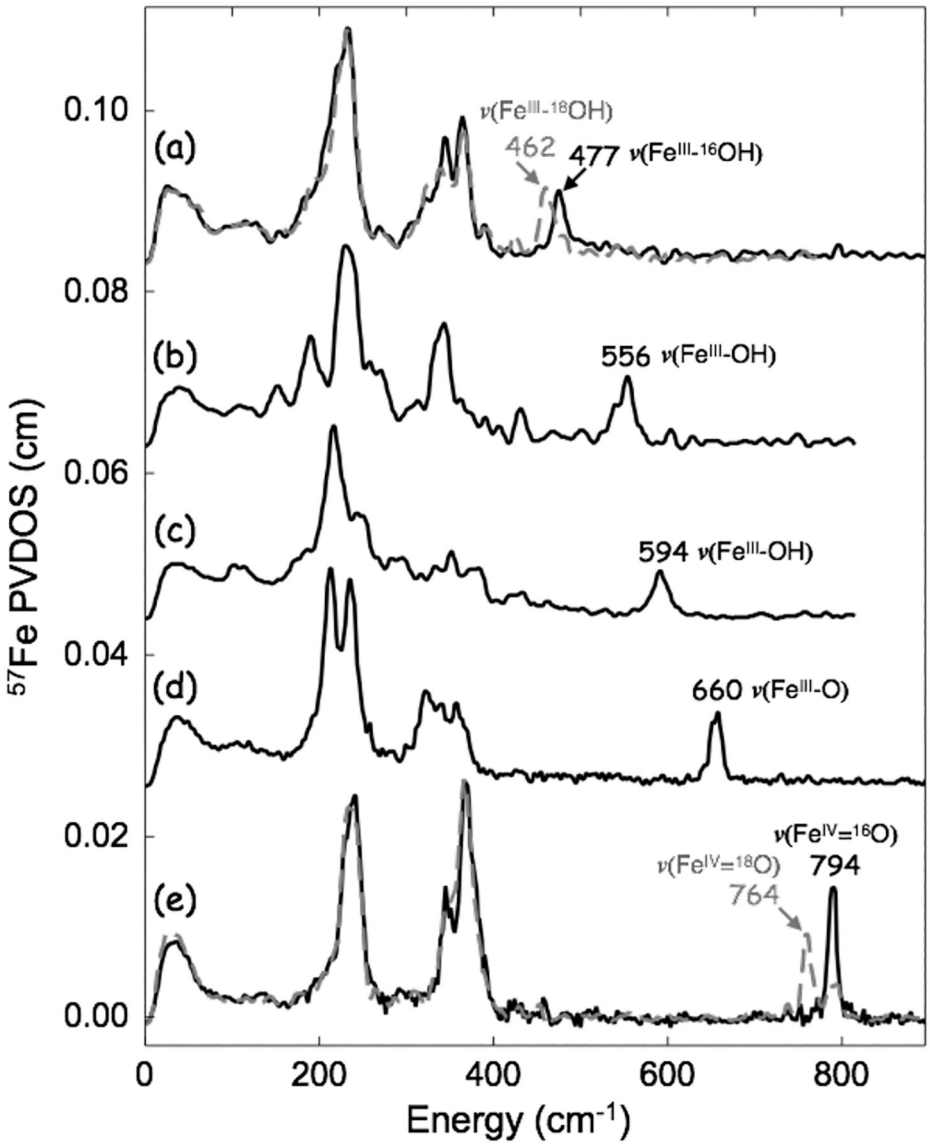

Figure 3.

^{57}Fe PVDOS spectra (black traces) of (a) [Fe^{III}{H$_3$buea}(OH))]$^{-}$, (b) [Fe^{III}{H$_2$pout}(OH)]$^{-}$, (c) [Fe^{III}{H$_3$bupa}(OH))]$^{-}$, (d) [Fe^{III}{H$_3$buea}(O)]$^{2-}$, and (e) [Fe^{IV}{H$_3$buea}(O)]$^{-}$. The spectra measured on the corresponding ^{18}O-atom labelled samples are shown with grey dash lines. The spectral features correspond to *ν*[Fe–O(H)] are indicated.

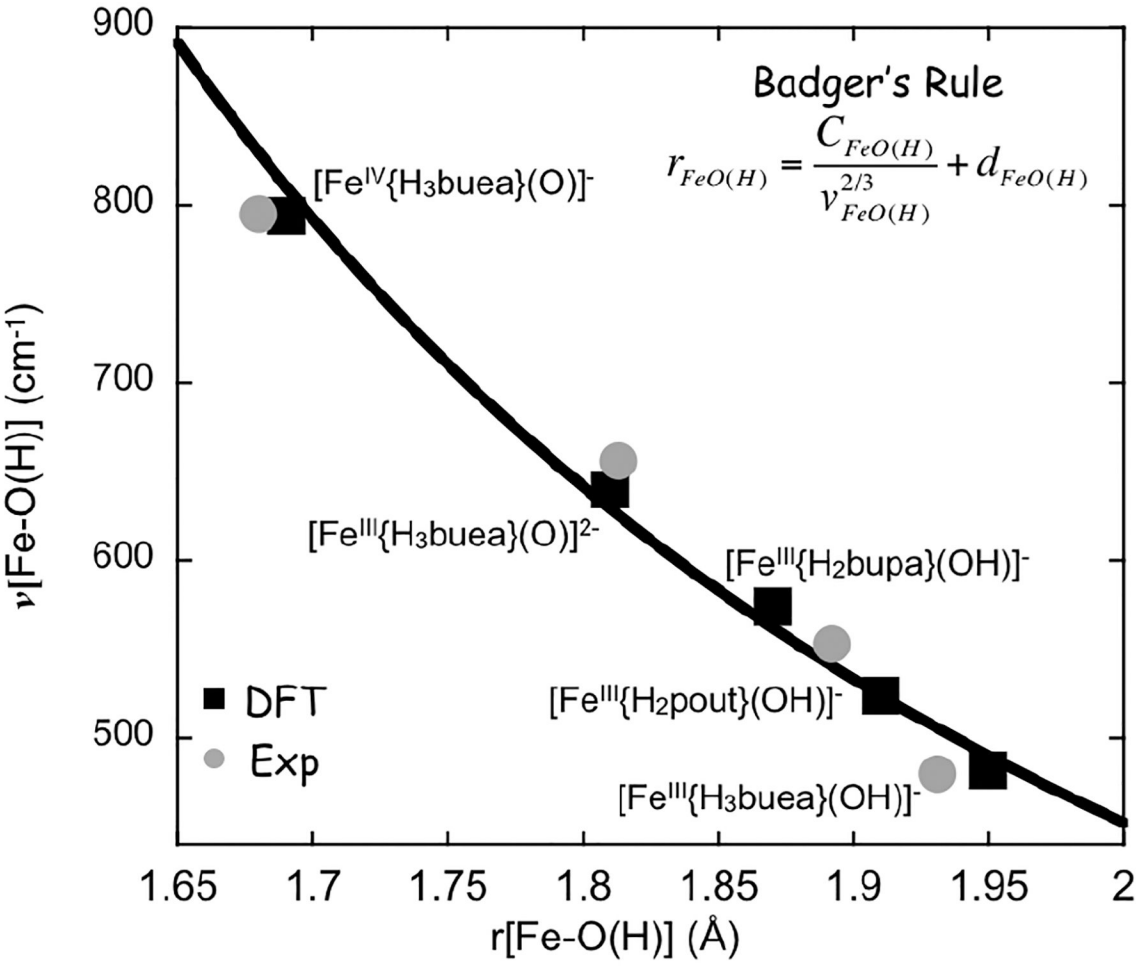

Figure 4.

The correlation plot between the Fe–O(H) bond length and its stretching frequency. The data points belong to different complexes are indicated in the figure. The experimentally and DFT obtained data points are shown in circles and squares, respectively. The black curve represents a fit to the DFT derived data using Badger's rule with the expression shown in the figure. The constants used for this fit are: $C_{\mathrm{FeO(H)}} = 56.692$, $d_{\mathrm{FeO(H)}} = 1.038$.